ACS APPLIED MATERIALS & INTERFACES

RESEARCH ARTICLE

www.acsami.org

Antibacterial Activity of Electrospun Polymer Mats with Incorporated Narrow Diameter Single-Walled Carbon Nanotubes

Jessica D. Schiffman* and Menachem Elimelech

Department of Chemical and Environmental Engineering, Yale University, New Haven, Connecticut 06520-8286, United States

Supporting Information

ABSTRACT: Polymer coatings featuring nonleaching antibacterial agents are needed to significantly reduce bacterial colonization and subsequent biofilm formation. Previously, single-walled carbon nanotubes (SWNTs) have been reported to be strong antimicrobial agents that kill microbes on contact. However, the antibacterial activity of freestanding polymer mats with a low weight percent of incorporated SWNTs has not been demonstrated. In this study, four different weight percents of well characterized, small diameter (0.8 nm) SWNTs were incorporated into electrospun polysulfone (PSf) mats. Electrospun PSf−SWNT mats were observed to be flexible and composed of continuous, cylindrical, and randomly oriented fibers. SEM micrographs revealed that SWNT ends were distributed along the longitudinal fiber axis. Loss of bacteria (*Escherichia coli*) viability was observed to directly correlate to increased SWNT incorporation within the mat, ranging from 18% for 0.1 wt % SWNTs to 76% for 1.0 wt % SWNTs. Time-dependent bacterial cytotoxicity studies indicated that the antimicrobial action of the PSf−SWNT mats occurs after a short contact time of 15 min or less. This study demonstrates the potential applicability of electrospun PSf−SWNT mats as antibacterial coatings.

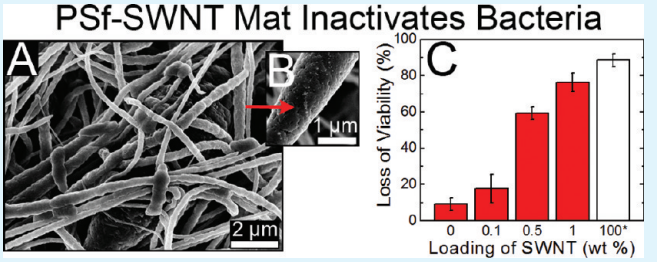

KEYWORDS: carbon nanotubes, electrospun, nanofibers, SWNT, SWCNT, toxicity

INTRODUCTION

Bacterial colonization and subsequent biofilm formation can occur on virtually any surface. On ship hulls, biofilm formation yields increased fuel consumption, whereas on biomedical implants and transcutaneous devices, it can facilitate the transmission of infectious diseases, which can be fatal.[1,2] Hence, there exists a high demand for robust antibacterial coatings that can be readily applied to a variety of surfaces.

One inexpensive, scalable processing method that can be utilized to fabricate such a flexible coating is electrospinning. Here, electrical forces are utilized to fabricate nonwoven mats comprising continuous nano- and macroscale diameter fibers that exhibit outstanding intrinsic structure−property relationships, notably high specific surface area and porosity.[3] Electrospinning can be applied to fabricate mats composed of a wide range of materials, such as synthetic and natural polymers, ceramics, and metals. Additionally, fabricated fiber mats can be tailored by many routes, for example by surface chemical modifications or incorporating species (e.g., nanoparticles and viruses) into the precursor spinning solution.[3−5] This versatility of composition makes electrospun mats ideal for use in a variety of industrial and biomedical applications.

Mats electrospun with incorporated antibacterial agents—quaternized chitosan,[6] silver,[7−9] titanium dioxide,[9] zinc oxide,[10] tetracycline hydrochloride,[11] *N*-halamines,[12] and chlorhexidine[13]—have demonstrated potential for use in biomedical applications, such as wound dressings, drug delivery platforms, and tissue engineering scaffolds. However, the exploitation of active antibacterial agents yields concerns related to their release rate, agent depletion, toxicity to human cells, and bacterial resistance.[14] To circumvent these problems, immobilized, nonleaching antibacterial agents that kill microbes on contact should be utilized.

Although most carbon-based nanomaterials are cytotoxic to bacteria,[15−18] single-walled carbon nanotubes (SWNTs) exhibit the highest toxicity.[19−21] Proposed cytotoxicity mechanisms include physical membrane perturbation and oxidative stress.[22,23] SWNT physiochemical properties—mainly dispersion/aggregation state, diameter, length, and electronic structure—influence their toxicity.[19,22,23] Several studies demonstrate the antibacterial properties of MWNTs and SWNTs in the form of suspended aggregates[20,21] or as deposit layers.[14,19,22,24] However, the use of either suspended or deposited carbonaceous nanomaterials as an antibacterial coating is limited by both practicality and cost.

The incorporation of small amounts of SWNTs into a polymer matrix holds a greater potential to serve as a nonleaching antibacterial coating. Recently, the toxicity of dip- and spin-coated SWNT-polymer films supported by glass substrates has been

Received: October 28, 2010
Accepted: January 2, 2011
Published: January 24, 2011

investigated.[14] Carbon blacks,[25,26] multiwalled carbon nanotubes (MWNTs),[23,27−30] and SWNTs[31−35] have been successfully incorporated into various electrospun polymers. These studies, however, focused on the carbon nanotube alignment and on the electronic, magnetic, or mechanical properties of the composite fibrous mats. Thus, the antibacterial activity of freestanding, flexible polymer-SWNT mats has yet to be demonstrated.

In this study, the antibacterial activity of SWNTs incorporated into electrospun polysulfone (PSf) fiber mats is investigated. We have utilized highly purified and well characterized narrow diameter SWNTs in order to relate the observed cytotoxicity to the SWNT physiochemical properties. The antibacterial activity of the fabricated PSf fiber mats to the Gram-negative bacteria, *Escherichia coli*, is evaluated as a function of the amount of SWNTs incorporated and bacteria-fiber mat contact time.

MATERIALS AND METHODS

Materials and Chemicals. Polysulfone (PSf) (M_w = 22 000 Da), dimethylformamide (DMF), and dimethyl sulfoxide (DMSO) were purchased from Sigma-Aldrich (St. Louis, MO). SWNTs (lot number SG65−000−0031), produced by the CoMoCAT process, were obtained from SouthWest NanoTechnologies, Inc. (Norman, OK). Company-published specifications on the SWNTs include: tube diameter of 0.8 ± 0.1 nm, carbon content >90% by weight, >50% of tubes are (6,5) chirality, >90% of tubes are semiconducting, and a Raman D-band to G-band ratio (D/G) of 0.960. Propidium iodide (PI) and 4′,6-diamidino-2-phenylindole (DAPI) were purchased from Invitrogen (Carlsbad, CA). Deionized water (DI) was obtained from a Milli-Q ultrapure water purification system (Millipore, Billerica, MA).

SWNT Purification. As-received SWNTs were refluxed in hydrochloric acid (37%) for 12 h followed by filtration with a 5-μm Omnipore membrane (Millipore). The carbon products were rinsed repeatedly with DI and the amorphous carbon was removed by oxidation at 350 °C for 6 h.

PSf−SWNT Mat Fabrication. PSf/DMF (4 g in 20 mL corresponding to 5 wt %) solutions were mixed for 24 h using a Tube Rotator (VWR, Bridgeport, NJ). Various amounts of SWNTs (0, 0.4, 20, and 40 mg, corresponding to 0, 0.1, 0.5, and 1.0 wt %, respectively) were added and sonicated continuously for 1 h using an ultrasonication probe (Misonix 3000, Misonix Inc., Farmingdale, NY). The PSf/DMF solution containing SWNTs was loaded into a BD Luer-Lok tip syringe (Becton, Dickinson & Co., Franklin Lakes, NJ). A Precision Glide 21-gauge needle (Becton, Dickinson & Co.) was attached to the syringe prior to securing it to an advancement pump (Harvard Apparatus, Plymouth Meeting, PA). Alligator clips were used to connect the positive anode of a high-voltage supply (Gamma High Voltage Research Inc., Ormond Beach, FL) to the needle and the negative anode to a copper plate wrapped in aluminum foil. The speed of the advancement pump, separation distance between the needle and collection plate, and applied voltage were held constant at 0.8 mL/h, 7 cm, and 20 kV, respectively.

Characterization. Raman spectra were acquired utilizing an excitation wavelength of 785 nm on an NRS-3100 instrument (Jasco) equipped with a confocal microscope. Thermo-gravimetric analysis (TGA) (SETSYS 16/18) was performed from 200 to 1000 °C at a heating rate of 10 °C/min. Average solution conductivity was determined from triplicate readings using a YSI Model 32 conductance meter (Yellow Springs Instrument Co., Inc., Yellow Springs, Ohio). Micrographs were acquired using a Hitachi ultra-high-resolution analytical field-emission scanning electron microscope (SEM) SU-70. An Emitech SC7620 sputtering machine was used to coat the surface of samples for 30 s with gold−platinum. Fiber diameter distribution was determined using ImageJ 1.41 software (National Institutes of Health, Bethesda, MD) by measuring the diameter of 50 random fibers from at least 5 different micrographs. Transmission electron microscopy (TEM) of as-received and purified SWNTs was conducted by NanoTEM Inc. (Phoenix, AZ).

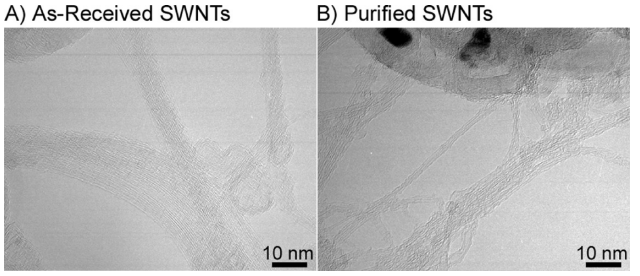

Figure 1. TEM micrographs of SWNTs (A) before and (B) after overnight purification using concentrated (37%) HCl solution.

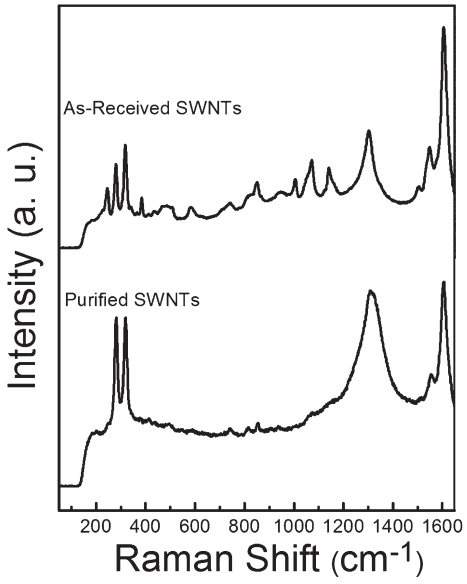

Figure 2. Raman spectra acquired using 785 nm excitation of as-received SWNTs and SWNTs after purification. Based on their radial breathing mode (RBM) peaks, purified SWNTs have diameters ranging from 0.88 to 0.78 nm.

Evaluation of Antibacterial Activity of Electrospun PSf-SWNT Mats. *Escherichia coli* (*E. coli*) K12 was grown in Luria−Bertani (LB) Broth medium at 37 °C and harvested in the midexponential growth phase. To remove residual macromolecules and other growth medium constituents, we washed cells twice and then resuspended them in an isotonic solution (0.9% NaCl, pH 5.7).

To study their toxicity to *E. coli*, we placed electrospun PSf−SWNT mats (25.4 mm × 25.4 mm) at the bottom of 51 mm^2 Petri dishes (Becton, Dickinson & Co., Franklin Lakes, NJ) to which the resuspended cells (10^7 cells/mL) in an isotonic solution (0.9% NaCl) were added. The toxicity of purified SWNTs was determined by preparing SWNT coatings as follows. About 2 mg of purified SWNTs were dispersed in 4 mL of DMSO and probe sonicated (Misonix 3000, Misonix Inc.) for 15 min. The suspension was then filtered through a mixed cellulose ester membrane filter (HABP, Millipore) to form a SWNT-coated filter. Next, 100 mL of ethanol was filtered through the membrane to remove residual DMSO, followed by 100 mL of 50% ethanol and 300 mL DI to remove the residual ethanol. Once cleaned, *E. coli* cells (10^6 cells/mL) were gently deposited by vacuum filtration onto the SWNT-coated filter, which was then transferred to separate Petri dishes. For all toxicity assays,

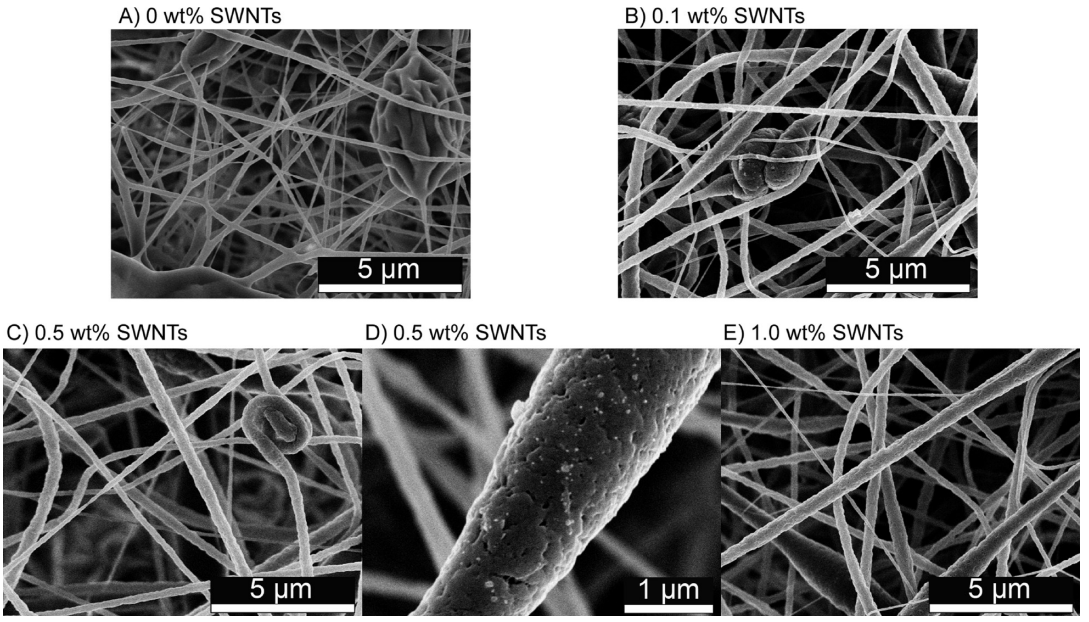

Figure 3. SEM micrographs displaying electrospun PSf mats containing (A) 0, (B) 0.1, (C, D) 0.5, and (E) 1.0 wt % loading of SWNTs. Images A−C and E display a 5 μm marker to demonstrate the overall fiber morphology. Image D displays a close-up image of a single large fiber containing dispersed SWNT bundles, with a 1 μm marker displayed.

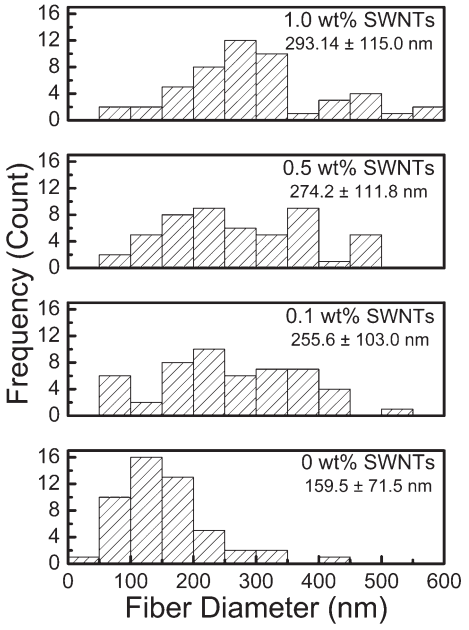

Figure 4. Fiber diameter distribution for mats electrospun from PSf containing 0, 0.1, 0.5, and 1.0 wt % initial loading of SWNTs as determined using ImageJ software on SEM micrographs. For each SWNT loading, the average fiber diameter and standard deviation of 50 random fiber diameters measured are also given.

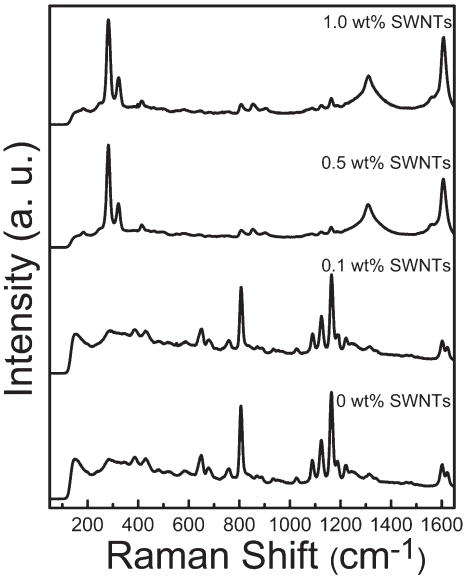

Figure 5. Raman spectra acquired using 785 nm excitation of PSf electrospun mats containing 0, 0.1, 0.5, and 1.0 wt % SWNTs.

E. coli cells were incubated at 37 °C for various times (15−60 min), depending on the experiment. No external forces were applied during incubation.

Viability loss was determined by a fluorescence assay as previously described.[19,22] Cells were stained in the dark with PI (excitation/emission at 535 nm/617 nm) for 15 min and then counter-stained with DAPI (excitation/emission at 358 nm/461 nm). Fluorescence images were acquired to detect the cells utilizing an epifluorescence microscope (Olympus) with a U filter (364 nm/440 nm). Ten representative images were taken at 200× magnification at various locations for each specimen. Dead cells and the total number of cells were determined by direct cell counting. The percentage of dead cells (or loss of viability) was determined from the ratio of the number of cells stained with PI divided by the number of cells stained with DAPI plus PI.

RESULTS AND DISCUSSION

SWNT Characteristics. To remove metal impurities and amorphous carbon, as-received SWNTs were purified using concentrated (37%) hydrochloric acid. Representative TEM micrographs (Figure 1) indicate that nanotubes were single walled and

bundled. After purification, SWNT sidewall structure remained intact and negligible metal impurities and amorphous carbon were visible. From thermogravimetric analysis (TGA) (see Figure S1 in the Supporting Information), it was determined that the purification procedure decreased the concentration of residual metal impurities from 1.9% for the as-received to 0.8% for the purified SWNTs.

Figure 2 displays the Raman spectra featuring the characteristic bands of both the as-received and purified SWNTs. The diameter of SWNTs can be determined utilizing the diameter-dependent frequency of the radial breathing mode (RBM), at $v <$ 400 cm^{-1}, wherein the tube diameter, $d = 248/v$. Purified SWNTs exhibited diameters ranging from 0.88 to 0.78 nm, which was a smaller diameter distribution than the as-received SWNTs (1.01 to 0.65 nm). This "narrowing" was most likely a result of the purification process, which removed the amorphous carbon and metal impurities. The diameter of the purified tubes is consistent with the specifications reported by the manufacturer (SouthWest NanoTechnologies, Inc.), namely $d = 0.8 \pm 0.1$ nm.

Two other characteristic bands are displayed in Figure 2: (i) the SWNT tangential mode or G-band at 1600 cm^{-1} that occurs because of the in-plane Raman-active mode in graphite and (ii) the SWNT disorder-induced D-band at 1350 cm^{-1}, which provides information about the crystalline quality of the samples. The D-band is representative of the degrees of structural disorder within the SWNTs.[31] From these bands, the D-band to G-band ratio (D/G), which is an empirical measure of purity, was determined to be 0.56 and 0.97 for as-received and purified SWNTs, respectively. These values are consistent with the D/G ratio (0.960) reported by the manufacturer (SouthWest Nano-Technologies, Inc.). The increase in the ratio indicates that the purification process increased the concentration of defects to the SWNTs.

PSf−SWNT Mat Characteristics. Polysulfone (PSf) was chosen to be the main constituent of all electrospun mats due to its high thermal and chemical stability.[36−39] Pure polymer mats were successfully electrospun from 5 wt % PSf solution (0 wt % SWNTs) and composed of fine, cylindrical fibers, with some beads also present (Figure 3A). The previously described, purified, debundled SWNTs were incorporated at various weight loadings (0.1, 0.5, and 1.0 wt %) by mechanical mixing into PSf solutions of the same composition (5 wt %). This aided in coating and dispersing the carbonaceous material.[31] The composite solutions were then successfully electrospun into fibrous PSf−SWNT mats (Figure 3). Even at low (0.1 wt %) loadings, dispersed SWNT bundles were apparent in SEM micrographs (Figure 3B). A close-up of SWNTs within an electrospun fiber containing 0.5 wt % SWNTs is presented in Figure 3D. This micrograph reveals that the surface morphology of individual PSf fibers is slightly rough, with some pitting present. Additionally, the dispersed SWNT bundles are prominently displayed as white spots on the close-up fiber.

All PSf−SWNT mats could be peeled away from the aluminum foil that covered the electrospinning target and were flexible. Visually, the color of the mats intensified with increasing SWNT incorporation. At 0 wt % SWNTs, PSf mats were white, whereas, at 0.1, 0.5, and 1.0 wt % SWNT loadings, they were off-white, light ash gray, and deep gray, respectively (see Figure S2 in the Supporting Information). Despite the visual changes, increasing the SWNT incorporation did not drastically alter the individual fibers within the mats. The concentration of beading seemed to decrease and, at 1.0 wt % SWNT loading, no beads were observed (Figure 3E). This finding was expected because increasing the electrospinning solution conductivity—e.g., by incorporating metal nanoparticles[40] or cationic salts[41,42]—has demonstrated the suppression of bead formation.[43] Our electrospinning solution conductivity increased upon SWNT incorporation, from 30 μS/cm for the PSf/DMF solution to 61 μS/cm after the addition of 1 wt % SWNTs, in agreement with previous studies.[27,30,35]

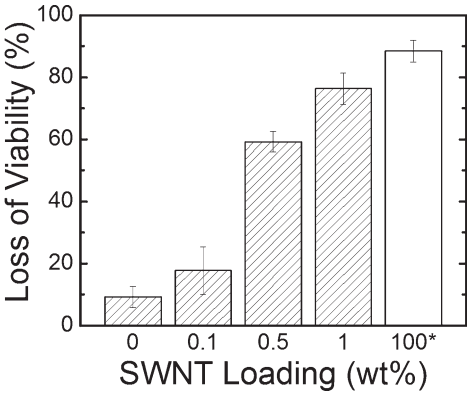

Figure 6. Fluorescence-based toxicity assay results for electrospun PSf mats containing 0, 0.1, 0.5, and 1.0 wt % SWNTs, as well as for a (100 wt %) SWNT-coated commercial filter. *E. coli* cells were incubated on the sample of interest for 1 h in an isotonic solution (0.9% NaCl, pH 5.7).

Average fiber diameters ($n = 50$) for the electrospun PSf−SWNT mats are displayed in Figure 4. Mats comprising pure PSf had an average fiber diameter of 159.5 ± 71.5 nm. At all wt % SWNTs incorporation concentrations, both the average and the range of fiber diameters increased. The diameters of electrospun fibers with 0.1, 0.5, and 1.0 wt % SWNT loading were on the same order at 255.6 ± 103.0 nm, 274.2 ± 111.8 nm, and 293.14 ± 115.0 nm, respectively. As previously noted, the incorporation of SWNTs into the electrospinning solution increases its conductivity, which, in turn, affects the fiber diameter.[31]

The presence of SWNTs within the electrospun PSf fibers was confirmed by Raman spectroscopy. Figure 5 displays the average spectra acquired on five different PSf mats electrospun with 0, 0.1, 0.5, and 1.0 wt % SWNT loading. At 0 and 0.1 wt % SWNT loading, only bands characteristic of PSf are displayed. At 807 cm^{-1} is the C−S−C symmetric stretch, which was previously assigned to out-of-plane benzene ring C−H deformation. The symmetric and asymmetric SO_2 stretching bands are located at 1088 and 1124 cm^{-1}, respectively, and the symmetric C−O−C stretching (1164 cm^{-1}) has the strongest intensity.[44−46] However, these four peaks become less prominent at 0.5 wt % SWNT loading, when the RBM, G-band, and D-band become evident. These peaks appear constant as the concentration of SWNTs increases from 0.5 to 1.0 wt %. In comparison to the spectra taken on SWNT powder (Figure 2), these three peaks are shifted to slightly higher frequencies when reinforced by the polymer matrix of the electrospun PSf. This observation could be attributed to interactions between the polymer and SWNTs[47] and is further supported by TGA. Our TGA data for electrospun PSf mats containing variable amounts of SWNTs indicate that the presence of SWNTs within the PSf mats shifts the degradation peaks to higher temperatures than those observed for either pure PSf mats or SWNTs alone (see Figure S3 in the Supporting Information).

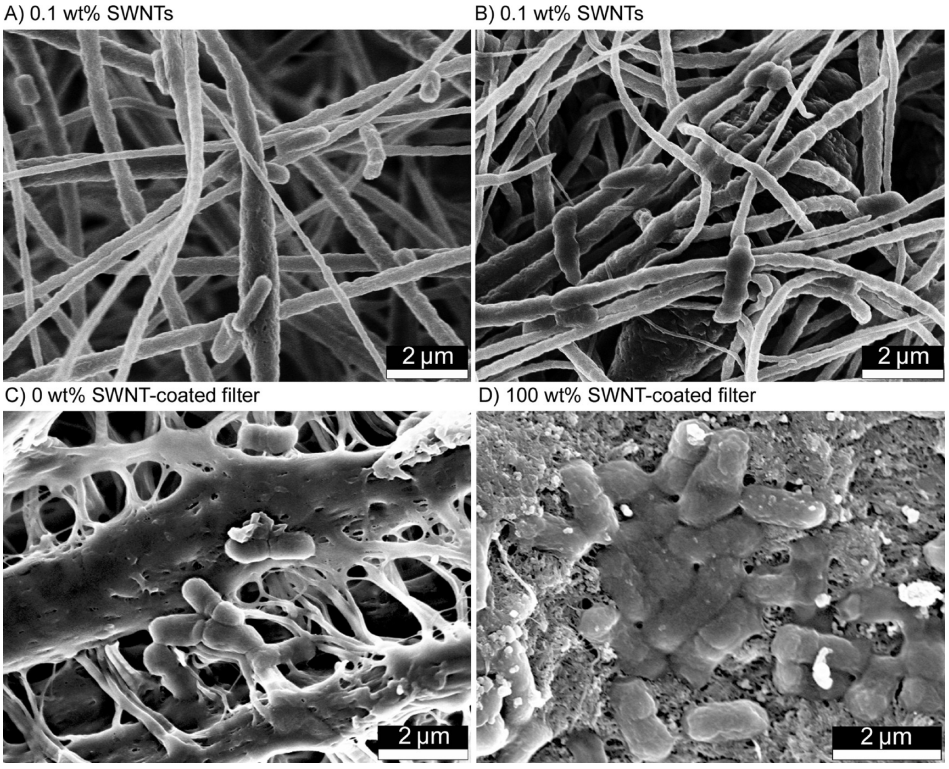

Figure 7. SEM micrographs displaying *E. coli* that have been incubated for 1 h on (A, B) PSf mats containing 0.1 wt % SWNTs and commercial filters coated with (C) 0 and (D) 100 wt % SWNT coating, respectively. Micrographs A and C display viable cells, whereas B and D display cells that have been inactivated by SWNTs.

Antibacterial Properties of PSf−SWNT Mats. The toxicity of electrospun PSf−SWNT mats to *E. coli* was evaluated using a fluorescence-based viability assay. Figure 6 indicates that bacteria inactivation after 1 h of contact with the test mats increased as a function of SWNT incorporation within the electrospun PSf mats. Control electrospun mats (0 wt % SWNTs) exhibited a 9 ± 4% inactivation rate of cells. Electrospun PSf−SWNT mats containing a low-SWNT loading (0.1 wt %) exhibited an average loss of cell viability of 18 ± 8%, whereas at the highest SWNT loading (1.0 wt %), the rate of inactivation was much higher, 76 ± 5%. This observation is likely a result of the increased presence, distribution, and likelihood of SWNT ends and bundles extending from the PSf fibrils and making direct contact with the bacteria.

Viable (Figure 7A) and inactivated bacteria (Figure 7B) show a distinct difference in cell morphology. The inactivated cells appear flattened and lose their cellular integrity, indicating they experienced irreversible cell damage and cell death.[22] The alignment of the *E. coli* along or perpendicular to the fiber axis might have some influence on cell inactivation. Perhaps at the lower weight percent SWNT loading, the cells that are touching multiple fibers have a greater chance of being in contact with fibers that contain exposed SWNT ends.

For comparison, the toxicity of commercial filters (i.e., control with no SWNTs) and commercial filters coated with 100 wt % purified SWNTs was also evaluated. The 100 wt % SWNT-coated commercial filters (Figure 6, solid white bar) exhibited slightly higher toxicity (88 ± 3%) than PSf mats loaded with 1.0 wt % SWNTs (76 ± 5%). These toxicity results are in agreement with previous experiments, wherein SWNT-coated filters, featuring SWNTs that measured 0.9 nm in diameter by 2 μm in length, exhibited an *E. coli* inactivation rate of 87 ± 7%.[22] Bacteria in contact with the SWNT-coated filters were both flattened and expanded (Figure 7D) compared to live cells on the control filters with no SWNTs that appeared healthy (Figure 7C). Bacteria exposed to the 100 wt % SWNT-coated filters are in contact with more SWNTs than when introduced to the electrospun low weight percent SWNT mats, which explains why they appear more flattened than those inactivated by the mats.

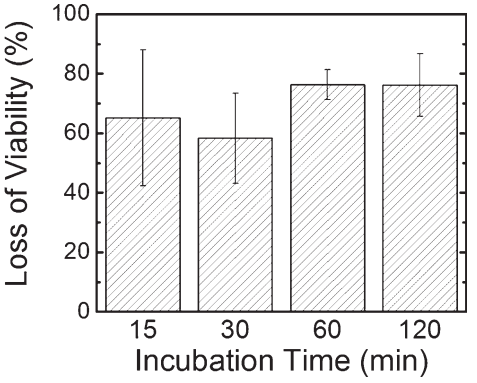

Figure 8. Fluorescence-based toxicity assay results as a function of incubation time for electrospun PSf mats containing 1.0 wt % SWNTs. *E. coli* was incubated on electrospun mats in an isotonic solution (0.9% NaCl, pH 5.7) at 37 °C.

Loss of viability as a function of time for mats electrospun from PSf solutions containing 1.0 wt % SWNTs is displayed in Figure 8. After 15 min of contact, the shortest time interval that can be tested using the fluorescence-based toxicity assay, high levels of

toxicity (65 ± 23%) were achieved. This percent of inactivation is not statistically different from the loss of viability observed after 2 h (76 ± 11%). These results are in agreement with our recent study concerning the bacterial toxicity of semiconducting SWNTs, where inactivation of *E. coli* did not increase beyond 15 min of incubation.[23]

CONCLUSION

Narrow-diameter SWNTs have been successfully incorporated into electrospun PSf fibrous mats. Regardless of the wt % of SWNTs incorporated, individual fibers within the composite mat are continuous, cylindrical, and randomly oriented. PSf−SWNT mats can be directly electrospun onto or applied as a conformal coating to any surface where bacterial colonization might occur. Increasing the SWNT loading within the electrospun mats directly correlates to increased toxicity of the fabricated mats. With 1.0 wt % SWNTs incorporated, electrospun PSf−SWNT mats exhibited nearly comparable toxicity to 100 wt % SWNT-coated filters. However, since antibacterial fibrous mats featuring a low weight percent of SWNTs can be applied as a thin coating to virtually any surface, they offer far greater versatility of application than uniform SWNT coatings.

ASSOCIATED CONTENT

Supporting Information. Thermo-gravimetric analysis (TGA) of as-received SWNTs (Figure S1); digital images of PSf mats electrospun at various SWNT loadings (Figure S2); TGA analysis of electrospun PSf membranes containing various loadings of SWNTs (Figure S3) (PDF). This material is available free of charge via the Internet at http://pubs.acs.org.

AUTHOR INFORMATION

Corresponding Author
*E-mail: jessica.schiffman@yale.edu.

ACKNOWLEDGMENT

We acknowledge the support of the National Science Foundation under Research Grant CBET- 0828795 and the Water-CAMPWS, a Science and Technology Center of Advanced Materials for the Purification of Water with Systems under the National Science Foundation Grant CTS-0120978.

REFERENCES

(1) Mattila-Sandholm, T.; Wirtanen, G. *Food Rev. Int.* **1992**, *8*, 573–603.
(2) Dunne, W. M., Jr. *Clin. Microbiol. Rev.* **2002**, *15*, 155–166.
(3) Schiffman, J. D.; Schauer, C. L. *Polym. Rev.* **2008**, *48*, 317–352.
(4) Greiner, A.; Wendorff, J. *Angew. Chem., Int. Ed.* **2007**, *46*, 5670–5703.
(5) Lee, S.-W.; Belcher, A. M. *Nano Lett.* **2004**, *4*, 387–390.
(6) Ignatova, M.; Starbova, K.; Markova, N.; Manolova, N.; Rashkov, I. *Carbohydr. Res.* **2006**, *341*, 2098–2107.
(7) Xu, X.; Yang, Q.; Wang, Y.; Yu, H.; Chen, X.; Jing, X. *Eur. Polym. J.* **2006**, *42*, 2081–2087.
(8) Rujitanaroj, P.-o.; Pimpha, N.; Supaphol, P. *Polymer* **2008**, *49*, 4723–4732.
(9) Son, B.; Yeom, B. Y.; Song, S. H.; Lee, C. S.; Hwang, T. S. *J. Appl. Polym. Sci.* **2009**, *111*, 2892–2899.
(10) Lee, S. *J. Appl. Polym. Sci.* **2009**, *114*, 3652–3658.
(11) Xu, X.; Zhong, W.; Zhou, S.; Trajtman, A.; Alfa, M. *J. Appl. Polym. Sci.* **2010**, *118*, 588–595.
(12) Tan, K.; Obendorf, S. K. *J. Membr. Sci.* **2007**, *305*, 287–298.
(13) Chen, L.; Bromberg, L.; Hatton, T. A.; Rutledge, G. C. *Polymer* **2008**, *49*, 1266–1275.
(14) Aslan, S.; Loebick, C. Z.; Kang, S.; Elimelech, M.; Pfefferle, L. D.; Tassel, P. R. V. *Nanoscale* **2010**, *2*, 1789–1794.
(15) Hu, W.; Peng, C.; Luo, W.; Lv, M.; Li, X.; Li, D.; Huang, Q.; Fan, C. *ACS Nano* **2010**, *4*, 4317–4323.
(16) Kang, S.; Mauter, M. S.; Elimelech, M. *Environ. Sci. Technol.* **2009**, *43*, 2648–2653.
(17) Lyon, D. Y.; Alvarez, P. J. J. *Environ. Sci. Technol.* **2008**, *42*, 8127–8132.
(18) Akhavan, O.; Ghaderi, E. *ACS Nano* **2010**, *4*, 5731–5736.
(19) Kang, S.; Pinault, M.; Pfefferle, L. D.; Elimelech, M. *Langmuir* **2007**, *23*, 8670–8673.
(20) Liu, S.; Wei, L.; Hao, L.; Fang, N.; Chang, M. W.; Xu, R.; Yang, Y.; Chen, Y. *ACS Nano* **2009**, *3*, 3891–3902.
(21) Arias, L. R.; Yang, L. *Langmuir* **2009**, *25*, 3003–3012.
(22) Kang, S.; Herzberg, M.; Rodrigues, D. F.; Elimelech, M. *Langmuir* **2008**, *24*, 6409–6413.
(23) Vecitis, C. D.; Zodrow, K. R.; Kang, S.; Elimelech, M. *ACS Nano* **2010**, *4*, 5471–5479.
(24) Rodrigues, D. F.; Elimelech, M. *Environ. Sci. Technol.* **2010**, *44*, 4583–4589.
(25) Hwang, J.; Muth, J.; Ghosh, T. *J. Appl. Polym. Sci.* **2007**, *104*, 2410–2417.
(26) Schiffman, J. D.; Blackford, A. C.; Wegst, U. G. K.; Schauer, C. L. *Carbohydr. Polym.* **2011**, doi: 10.1016/j.carbpol.2011.01.013.
(27) Lu, P.; Hsieh, Y.-L. *ACS Appl. Mater. Interfaces* **2010**, *2*, 2413–2420.
(28) Ge, J. J.; Hou, H.; Li, Q.; Graham, M. J.; Greiner, A.; Reneker, D. H.; Harris, F. W.; Cheng, S. Z. D. *J. Am. Chem. Soc.* **2004**, *126*, 15754–15761.
(29) Sung, J. H.; Kim, H. S.; Jin, H.-J.; Choi, H. J.; Chin, I.-J. *Macromolecules* **2004**, *37*, 9899–9902.
(30) McCullen, S. D.; Stano, K. L.; Stevens, D. R.; Roberts, W. A.; Monteiro-Riviere, N. A.; Clarke, L. I.; Gorga, R. E. *J. Appl. Polym. Sci.* **2007**, *105*, 1668–1678.
(31) Ayutsede, J.; Gandhi, M.; Sukigara, S.; Ye, H.; Hsu, C.-M.; Gogotsi, Y.; Ko, F. *Biomacromolecules* **2006**, *7*, 208–214.
(32) Sen, R.; Zhao, B.; Perea, D.; Itkis, M. E.; Hu, H.; Love, J.; Bekyarova, E.; Haddon, R. C. *Nano Lett.* **2004**, *4*, 459–464.
(33) Gao, J.; Yu, A.; Itkis, M. E.; Bekyarova, E.; Zhao, B.; Niyogi, S.; Haddon, R. C. *J. Am. Chem. Soc.* **2004**, *126*, 16698–16699.
(34) Salalha, W.; Dror, Y.; Khalfin, R. L.; Cohen, Y.; Yarin, A. L.; Zussman, E. *Langmuir* **2004**, *20*, 9852–9855.
(35) Liu, Y.; Gilmore, K. J.; Chen, J.; Misoska, V.; Wallace, G. G. *Chem. Mater.* **2007**, *19*, 2721–2723.
(36) Wang, Z.-G.; Wang, J.-Q.; Xu, Z.-K. *J. Mol. Catal. B: Enzym.* **2006**, *42*, 45–51.
(37) Gopal, R.; Kaur, S.; Feng, C. Y.; Chan, C.; Ramakrishna, S.; Tabe, S.; Matsuura, T. *J. Membr. Sci.* **2007**, *289*, 210–219.
(38) Yongyi, Y.; Puxin, Z.; Hai, Y.; Anjian, N.; Xushan, G.; Dacheng, W. *Front. Chem. China* **2006**, *1*, 1673–3495.
(39) Li, G.; Li, P.; Yu, Y.; Jia, X.; Zhang, S.; Yang, X.; Ryu, S. *Mater. Lett.* **2008**, *62*, 511–514.
(40) Saquing, C. D.; Manasco, J. L.; Khan, S. A. *Small* **2009**, *5*, 944–951.
(41) Lin, T.; Wang, H.; Wang, H.; Wang, X. *Nanotechnology* **2004**, *15*, 1375.
(42) Arayanarakul, K.; Choktaweesap, N.; Aht-ong, D.; Meechaisue, C.; Supaphol, P. *Macromol. Mater. Eng.* **2006**, *291*, 581–591.
(43) Thompson, C. J.; Chase, G. G.; Yarin, A. L.; Reneker, D. H. *Polymer* **2007**, *48*, 6913–6922.
(44) Kim, H. J.; Fouda, A. E.; Jonasson, K. *J. Appl. Polym. Sci.* **2000**, *75*, 135–141.

(45) Ellis, G.; Sanchez, A.; Hendra, P. J.; Willis, H. A.; Chalmers, J. M.; Eaves, J. G.; Gaskin, W. F.; Krüger, K. N. *J. Mol. Struct.* **1991**, *247*, 385–395.
(46) Gordeyev, S. A.; Nikolaeva, G. Y.; Prokhorov, K. A.; Withnall, R.; Dunkin, I. R.; Shilton, S. J.; Pashinin, P. P. *Laser Phys.* **2001**, *11*, 82–85.
(47) Ramanathan, T.; Liu, H.; Brinson, L. C. *J. Polym. Sci., Part B: Polym. Phys.* **2005**, *43*, 2269–2279.